MULTIFUNCTIONAL GOLD-SILICA COMPOSITE PLATFORM TOWARDS COMPREHENSIVE CANCER THERAPY

TEW LIH SHIN

UNIVERSITI SAINS MALAYSIA

2018

MULTIFUNCTIONAL GOLD-SILICA COMPOSITE PLATFORM TOWARDS COMPREHENSIVE CANCER THERAPY

by

TEW LIH SHIN

Thesis submitted in fulfillment of the requirements
for the degree of
Master of Science

August 2018

ACKNOWLEDGEMENT

First and foremost, I would like to express my sincere gratitude to my supervisor Dr. Siti Hawa Ngalim for the support, encouragements and guidance throughout the work on this thesis. Thanks for sharing your knowledge on this exciting field of research and your valuable contributions during the writing process. I appreciate the time you had given me in your extremely busy schedules. I am especially grateful to Dr Vuanghao Lim for their valuable comments and suggestions for the research works. I am also thankful to Dr Yit Lung Khung and Dr Nai Tzu Chen for providing me all the facilities required for synthesis and characterisation and supporting me during my stay at Taiwan.

During my postgraduate studies, I have been fortunate enough to work with a great team of people. I wish to acknowledge and thank Tsung Hsi Lee for being one of the most helpful person in running experiments. I am highly grateful to Joline Tung, my biggest supporter for the stimulating discussions and insightful comments. I would also like to thank Irene Tung and Meng Tung Cai for their support. Without their help, I could not have completed this work.

Last but not least, I thank my friends and family members, who have supported me wholeheartedly through this process, without them I would not have accomplished this work.

TABLE OF CONTENTS

ACKNOWLEDGEMENT ii

TABLE OF CONTENTS iii

LIST OF TABLES vii

LIST OF FIGURES viii

LIST OF ABBREVIATIONS xi

LIST OF SYMBOLS xiv

ABSTRAK xv

ABSTRACT xvii

CHAPTER 1 - INTRODUCTION

1.1 Objectives of the study 6

1.1.1 General objectives 6

1.1.2 Specific objectives 7

CHAPTER 2 - LITERATURE REVIEW

2.1 Gold nanoshells (GNS) 9

2.2 Mesoporous silica nanoparticles (MSNs) as drug carriers 12

2.3 Target scheme - antibodies, peptide & aptamer (Apt) 15

2.3.1 Aptamer (Apt) 16

2.4 Doxorubicin 18

2.5 Principle of two-photon excitation (TPE) 21

2.5.1 Photothermal therapy (PTT) 23

2.5.2 Controlled release 25

CHAPTER 3 - METHODOLOGY

3.1 Chemical reagents and media 29

3.2 Preparation of amino-functionalised mesoporous silica nanoparticles (MSN-NH_2) 30

3.2.1 Doxorubicin (DOX) loading 32

3.3 Gold Nanoshell (GNS) synthesis 33

3.4 Surface functionalisation of GNS 34

3.5 Two photon induced photoluminescence (TPIP) and photostability of gold nanoshell (GNS) 37

3.6 Photothermal profile of GNS 38

3.7 Cytotoxicity assay of DOX-GNS-PEG-Apt 38

3.8 Analysis of target specificity 39

3.9 Inductively coupled plasma mass spectrometry (ICP-MS) sample preparation 40

3.10 *In vitro* cytotoxicity of GNS alone and loaded with DOX with two photon irradiation 41

CHAPTER 4 - RESULTS AND DISCUSSION

4.1 Synthesise, functionalise and characterisation of MSNs coated with a layer of gold shell (GNS) 45

4.1.1 Characterisation of mesoporous silica nanoparticles (MSNs) 46

4.1.2 Formation of gold nanoshell (GNS) 48

4.1.3 Doxorubicin (DOX) loading capacity 52

4.1.4 Surface modification 55

4.2 Demonstration of two photon excitation (TPE) triggered gold nanoshell deformation *via* UV-VIS spectroscopy and TEM 56

4.2.1 Photoluminesence and photostability of GNS 56

4.3 Evaluation of the photothermal efficacy 60

4.3.1 Photothermal therapy (PTT) profile 60

4.4 *In vitro* studies 61

4.4.1 Cytotoxicity assay DOX-GNS-PEG-Apt 61

4.4.2 Analysis of target specificity 63

4.4.3 *In vitro* two photon excited PTT and controlled release 65

4.4.4 Immunofluorescence staining.....72

CHAPTER 5 - CONCLUSION

5.1 Conclusion 74

5.2 Future studies 76

REFERENCES.....77

APPENDICES

LIST OF TABLES

		Page
Table 3.1	List of chemical reagents and media used in this study	29
Table 3.2	Variety K-gold to seed ratio were tried to optimise the condition for complete gold shell formation.	34
Table 3.3	Sequence of amino-labelled AS1411 Apt	36
Table 4.1	Various concentrations of DOX from 1.95 to 125 µg/mL were prepared and the absorbance values were determined at 480 nm wavelength	52
Table 4.2	The absorbance value for supernatants after centrifugation.	54
Table 4.3	Encapsulation efficiency and content of DOX in MSNs-NH_2.	55

LIST OF FIGURES

		Page
Figure 1.1	Multifunctional and cargo loading of mesoporous silica nanoparticles (MSNs)	5
Figure 2.1	Theoretically calculated optical resonance of GNS over a range of core radius/shell thickness ratio	11
Figure 2.2	A controlled drug release nanosystem *via* chemical stimulus was designed by Lai and colleagues	14
Figure 2.3	Schematic diagram of Apt folded into three-dimensional conformations	16
Figure 2.4	Chemical structure of Doxorubicin (DOX)	19
Figure 2.5	Jablonski (energy level) diagram of (a) single photon excitation and (b) two photon excitation	22
Figure 2.6	The overall process of photo-thermal conversion upon laser irradiation	24
Figure 2.7	SKBr3 Breast cancer cells (left) and MCF-7 breast carcinoma cells (right) were seeded side by side on coverslip. Within the laser spot which outlined in white, SKBr3 breast cancer cells incubated with anti HER2-conjugated GNS undergone morbidity while the viability of MCF-7 breast carcinoma cells remained	25
Figure 3.1	Diagram for mesoporous silica nanoparticles (MSNs) synthesis	31
Figure 3.2	Area of MSNs were selected for size analysis	32
Figure 3.3	Graphical illustration of (i) SH-PEG2k-NHS and (ii) amino-labelled AS1411 aptamer conjugation on DOX-GNS	35
Figure 3.4	Two photon microscopy system with Chameleon Discovery dual laser output	37
Figure 3.5	Location of cells that were viewed under confocal microscope	40
Figure 3.6	Location of cells that were viewed under confocal microscope.	43

Figure 4.1	Schematic illustration of GNS synthesis route *via* growth-mediated process	45
Figure 4.2	TEM images of MSNs synthesised *via Stöber* process. The magnification for MSNs was at (a) 20,000X and (b) 400,000X. (c) The determination average particle size of MSNs was 84.90 ± 10.9 nm based on the histogram functions for the size analysis of MSNs	46
Figure 4.3	FTIR spectra of synthesised MSNs, extracted MSNs and MSN-NH_2	47
Figure 4.4	TEM images of gold colloids (a) with average particle diameter of 2.10±0.48 nm prepared using THPC as a reducing agent. (b) Plasmon absorption spectra of THPC-gold nanoparticle measured every other day for three weeks	49
Figure 4.5	TEM images of (a) gold colloids seeded on MSNs (seeds). Growth of gold nanoshell (GNS) with different ratio K-gold to seed (b) 1:1 (c) 2:1 (d) 3:1 (e) 4:1 and (f) 5:1	50
Figure 4.6	Plasmon absorption spectra of gold colloids, seed and gold nanoshell with different ratios of K-gold to seed (b) 1:1 (c) 2:1 (d) 3:1 (e) 4:1 and (f) 5:1	51
Figure 4.7	DOX standard curve used for calculation of drug loading efficiency. Various concentration of DOX from 1.95 to 125 µg/mL was prepared and the absorbance value was determined at 480 nm wavelength	53
Figure 4.8	FTIR spectra of GNS, GNS-PEG and GNS-PEG-Apt	55
Figure 4.9	(a) Absorption of GNS before (▪) and after (•) two photon irradiation. TEM images and EDX line scanned elemental profiles of GNS before (b,d) and after (c,e) two photon irradiation at 850 nm. The red line in EDX profile refers to silica element while the blue line refers to the gold element.	57
Figure 4.10	TEM images of GNS reshaping after irradiated with TPE.	58
Figure 4.11	The TPIP profiles of GNS under exposure with 0.5 % and 1 % of TPE power respectively.	59
Figure 4.12	Temperature change (ΔT) for water (control) and GNS in aqueous solution at 0.5, 1.0 and 1.5 mg/ml under laser irradiation.	60

Figure 4.13	Cell viability test on MDA-MB-231 cells with GNS-PEG-Apt at the concentration of 25, 50, 75 and 100 μg/ml	62
Figure 4.14	Confocal microscopy on MCF-10A cells (1st row) and MDA-MB-231 cells (2nd row) after 2 hours incubation (a,f) without and with Cy5-tagged AS 1411 aptamer at concentration of (b,g) 17, (c,h) 34, (d,i) 51 and (e,j) 68 pmoles. Scale bar is 10 μm.	64
Figure 4.15	Cellular uptake of GNS-PEG and GNS-PEG-Apt by MDA-MB-231 cells.	65
Figure 4.16	Time lapse fluorescence microscopy images showed the performance of dual therapy in control (a), GNS-PEG-Apt (b) and DOX-GNS-PEG-Apt (c) incubated with MDA-MB-231 cells under 12 mW repetitive laser irradiation.	67
Figure 4.17	Time lapse fluorescence microscopy images showed the performance of dual therapy in control (a), GNS-PEG-Apt (b) and DOX-GNS-PEG-Apt (c) incubated with MDA-MB-231 cells under 24 mW repetitive laser irradiation.	68
Figure 4.18	Time lapse fluorescence microscopy images showed the performance of dual therapy in control (a), GNS-PEG-Apt (b) and DOX-GNS-PEG-Apt (c) incubated with MDA-MB-231 cells under 38 mW repetitive laser irradiation.	69
Figure 4.19	Time lapse fluorescence microscopy images showed the performance of dual therapy in control (a), GNS-PEG-Apt (b) and DOX-GNS-PEG-Apt (c) incubated with MDA-MB-231 cells under 46 mW repetitive laser irradiation.	70
Figure 4.20	Time lapse fluorescence microscopy images showed the performance of dual therapy in control (a), GNS-PEG-Apt (b) and DOX-GNS-PEG-Apt (c) incubated with MDA-MB-231 cells under 55 mW repetitive laser irradiation.	71
Figure 4.21	Fluorescence intensity of YO-PRO-1 as a function of irradiation period for the three conditions was plotted at different output laser of powers.	72
Figure 4.22	Immunofluorescence staining of caspase-3 (green) in control GNS-PEG-Apt and DOX-GNS-PEG-Apt incubated with MDA-MB-231 cells.	74

LIST OF ABBREVIATIONS

Apt	Aptamer
APTES	3-aminopropyltriethoxysilane
AuNP	Gold nanoparticle
Au-S	Gold-sulfur bond
CdS	Cadmium sulfide
CTAB	Hexadecyltrimethylammoniumbromide
CW	Continuous wave
DEPC	Diethylpyrocarbonate
DLS	Dynamic Light Scattering
DNQ	2-diazo-1,2-naphthoquinones
DOX	Doxorubicin
DTX	Docetaxel
EDX	Energy Dispersive X-ray spectroscopy
FBS	Foetal bovine serum
FDA	Food and Drug Administration
FTIR	*Fourier*-transform infrared spectroscopy
GNS	Gold nanoshell

$HAuCl_4$	Chloroauric acid
HepG2 cells	Human liver carcinoma cells
ICP-MS	Inductively coupled plasma mass spectrometry
K_2CO_3	Potassium carbonate
LSPR	Localised surface plasmon resonance
MCM-41	Mobile crystalline material-41
MSNs	Mesoporous silica nanoparticles
MSN-NH_2	Amino-terminated mesoporous silica nanoparticle
NaOH	Sodium hydroxide
NH_4OH	Ammonium hydroxide
NH_4NO_3	Ammonium nitrate
NHS	N-hydroxylsuccinimide
NIR	Near infrared
PBS	Phosphate buffered saline
PS	Penicillin-streptomycin
PTT	Photothermal therapy
ROS	Reactive oxygen species
SH-PEG-NHS	Thiol-polyethylene glycol-succinimidyl ester

SPR	Surface plasmon resonance
STEM	Scanning transmission electron microscope
TEOS	Tetraethoxysilane
TEM	Transmission Electron Microscopy
THPC	Tetrakis(hydroxymethyl)phosphonium chloride
TPE	Two photon excitation
TPIP	Two photon induced photoluminescence
UV-Vis	Ultraviolet-visible spectroscopy
WGA-488	Wheat germ agglutinate AlexaFluor 488

LIST OF SYMBOLS

∅	Diameter
%	Percentage
°C	Degree Celsius
g	Gram
M	Molar
MHz	Megahertz
mg/ml	Milligram per millilitre
ml	Millilitre
mM	Millimolar
nm	Nanometre
U/ml	Units per millilitre
µl	Microlitre
µg/ml	Microgram per milliliter
x g	Gravity at the Earth's surface
§	Section
ΔT	Temperature change

KOMPOSIT MULTIFUNGSI EMAS-SILIKA KE ARAH TERAPI KANSER KOMPREHENSIF

ABSTRAK

Pembasmian sel kanser yang tidak menyeluruh berdasarkan rawatan tunggal kemoterapi atau terapi radiasi seringkali dilaporkan. Justeru, peranti nano berasaskan nanokulit emas mula diminati kerana kebolehubahan teras dan lapisan biofungsi juga resonans plasmon permukaan tempatan (LSPR) daripada gelombang cahaya nampak ke inframerah (NIR) yang sesuai untuk aplikasi biomedikal. Dalam projek ini, nanokulit emas (GNS), yang berteraskan nanopartikel silika mesoliang (MSN) berisi doxorubicin (DOX) serta polietilina glikol (PEG) dan AS1141 aptamer (Apt) pada lapisan luar (DOX-GNS-PEG-Apt), telah direka untuk terapi pengaktifan kimia dan fototerma menggunakan laser dua foton. Teras MSN disintesis melalui proses *Stöber* diikuti dengan pengisian DOX dan akhirnya tumbesaran lapisan emas pada permukaan MSN melalui proses pengantara pertumbuhan. Seterusnya, PEG dan Apt dikonjugat pada GNS. GNS yang disintesiskan dan pengubahsuaian permukaannya telah dicirikan menggunakan Transformasian *Fourier* Inframerah (FTIR), spektroskopi Ultraungu-Nampak (UV-Vis) dan Mikroskop Penghantaran Elektron (TEM). Keputusan menunjukkan 30.00 ± 2.91 % doxorubisin (DOX) telah dimuatkan ke dalam MSN. GNS yang disintesis kemudiannya dianalisa menggunakan UV-Vis dan TEM, dimana nisbah 4:1 K-emas kepada bijian MSN-NH_2 menghasilkan ketebalan emas yang sesuai. Nanopartikel dengan liputan emas lengkap pada teras silika mesoliang diperhatikan dan spektra penyerapan plasmon memuncak pada 800 nm. Berdasarkan data TEM dan Tenaga Penyebaran Sinar X (EDX),

filem emas yang disintesis melalui proses pengantara pertumbuhan adalah sekitar 10 - 15 nm tebalnya. Kemudian, eksitasi dua foton (TPE) diperkenalkan untuk menilai keberkesanan terapi phototerma (PTT) sahaja dan terapi sinergi kimia dan fototerma. Kecacatan GNS berlaku selepas pendedahan selama 10 saat kepada TPE pada gelombang 850 nm, lalu membolehkan pelepasan dadah kemoterapi terkawal dari rongga mesoliang. Kecacatan GNS dibuktikan dengan penganjakan puncak resonans plasmon dari 800 ke 570 nm dan morfologi bagi GNS selepas TPE disahkan lagi dengan TEM. Menurut kajian *in vitro*, DOX-GNS-PEG-AS1141 melekat secara selektif pada sel MDA-MB-231 (kanser) tetapi tidak pada sel MCF-10A (bukan kanser), kerana sel-sel kanser mempamerkan banyak reseptor nukleolin yang boleh melekat pada AS1141. Penggunaan DOX-GNS-PEG-AS1141 sahaja tanpa PTT juga tidak sitotoksik; kefahaman sel MDA-MB-231 apabila dirawat sehingga 100 μg/mL DOX-GNS-PEG-AS1141 tidak jauh berbeza dengan kawalan negatif. Sebaliknya, sel MDA-MB-231 yang dikenakan terapi sinergi kimia-fototerma terapi bersama DOX-GNS-PEG-Apt selepas TPE mempamerkan intensiti pendarfluor YO-PRO yang lebih tinggi, 8.38 ± 2.11 kali ganda apabila terdedah kepada TPE pada 850 nm dengan kuasa output 55 $mW/\mu m^2$, berbanding rawatan PTT sahaja dengan GNS-PEG-Apt yang memaparkan kenaikan 6.89 ± 2.05 kali. Hasil ini menunjukkan terapi sinergi kimia-fototerma merupakan terapi yang berkesan. Kesimpulannya, GNS adalah nanoplatform yang boleh menjanjikan gabungan teknik pelepasan dadah terkawal bersama-sama terapi fototerma.

MULTIFUNCTIONAL GOLD-SILICA COMPOSITE PLATFORM TOWARDS COMPREHENSIVE CANCER THERAPY

ABSTRACT

Incomplete cancer cells eradication with sole treatment of chemotherapy or radiation therapy was commonly reported. Therefore, gold nanoshells-based nanodevices have gained interests owing to the tuneablity of the localised surface plasmon resonance (LSPR) from visible to near infrared (NIR) wavelength, which is favourable for biomedical applications. In this work, gold nanoshell (GNS), of which has mesoporous silica nanoparticle core (MSN) filled doxorubicin (DOX) as well as polyethylene glycol (PEG) and AS1141 aptamer (Apt) at the outer layer (DOX-GNS-PEG-Apt), was designed for two photon laser-triggered chemo- and photothermal therapy. The results show 30.00 ± 2.91 % of doxorubicin (DOX) was loaded into MSNs. The synthesised GNS was then analysed by UV-Vis spectroscopy and TEM, of which 4:1 ratio of K-gold to MSN-NH_2 seed produced ideal gold thickness. The nanoparticles with a complete gold coverage on mesoporous silica core were observed. Based on the TEM and Energy Dispersive X-Ray spectroscopy (EDX) data, the gold film synthesised *via* grow-mediated process was approximately 10 – 15 nm thickness. Then, two photon excitation (TPE) was introduced to evaluate the efficacy of photothermal therapy (PTT) alone and the synergistic chemo-photothermal therapy. Deformation of GNS was evidenced by the blue shift of plasmon resonance peak from 800 to 570 nm and the morphology of the GNS after TPE was further confirmed with TEM. According to the *in vitro* study, DOX-GNS-PEG-Apt positive selectively bound to MDA-MB-231 cells (cancerous) but not MCF-10A cells (non-cancerous). In this work, synergistic chemo-photothermal therapy with DOX-GNS-PEG-

Apt treated MDA-MB-231 cells after TPE exhibited higher YO-PRO-1 fluorescence intensity，8.38 ± 2.11 folds with output power at 55 mW/μm^2, as compared to PTT alone with GNS-PEG-Apt which only exhibited 6.89 ± 2.05 fold increment. This result demonstrated synergistic chemo-photothermal therapy exhibited a better therapy. Taken together, GNS is a promising nanoplatform for dual controlled drug release and photothermal therapy approach.

CHAPTER 1

INTRODUCTION

Nanotechnology opens a new avenue towards successful cancer diagnosis and treatment, and astounding results in clinical trials have been reported. There are several comprehensive reviews available on the challenges and opportunities of nanotechnology for cancer therapy (Friberg and Nystrom, 2015, Wicki et al., 2015, Kobayashi and Lin, 2006, Kawasaki and Player, 2005). It is recognised that nanotechnology exhibits the potential in replacing current cancer treatments due to the ability for specific targeting (Climent et al., 2012, Li et al., 2012a). Antibody or short peptide conjugated on drug-loaded nanoparticles selectively target specific cell surface receptor on cancer cells; ultimately, sufficient dosage of chemotherapeutic drug is delivered to cancer cells while limiting toxicity in healthy cells. Thus, a high dosage of drug is not required to exert the same or even better efficacy, which ultimately reduces the cost of treatment. Also, the ability of chemotherapeutic drug to be controlled released by external (light, magnetic field and ultrasound) (Rodzinski et al., 2016, Ge et al., 2012, Angelatos et al., 2005) or internal (pH, temperature) (Lee et al., 2010, Liu et al., 2010, Angelos et al., 2009, Du et al., 2009, Zhang and Misra, 2007, Huang et al., 2004) stimuli reduces the chances of premature drug release during its transport. Application of nanotechnology in curing cancer cells has other advantages over conventional cancer therapy including prolonged circulation time and enhanced solubility of chemotherapeutic drugs.

Several types of nanosystems including metallic nanoparticle (Baffou and Quidant, 2013, Ahmad et al., 2010, Kogan et al., 2007), polymer nanoparticle (Du et al., 2011, Tang et al., 2009, Mukerjee and Vishwanatha, 2009, Tong and Cheng, 2007), silica nanoparticle (Argyo et al., 2014, Zhang et al., 2012, Lee et al., 2011, Yu et al., 2011, Liu et al., 2009), quantum dot (Delehanty et al., 2009, Medintz et al., 2005, Michalet et al., 2005), liposome (Allen and Cullis, 2013, Chang and Yeh, 2012, Harris et al., 2002, Batist et al., 2001), dendrimer (Wolinsky and Grinstaff, 2008, Tomalia et al., 2007, Majoros et al., 2006, Majoros et al., 2005, Malik et al., 1999) and carbon nanotube (Kostarelos et al., 2009, Liu et al., 2008, Kam et al., 2005) were developed. Among the mentioned nanosystems, gold nanoparticles (AuNP) have drawn wide attention from numerous researchers due to their inherent attributes such as chemical stability and excellent optical properties. Also, AuNP has high photothermal efficiency thanks to localised surface plasmon resonance (LSPR) that make AuNP nanostructures as an attractive platform for biomedical applications (Jain et al., 2006, Link and El-Sayed, 2000, Elghanian et al., 1997). Au possesses an excellent oxidation resistance which does not interfere with its usability under atmospheric conditions thus making it an outstanding candidate for both *in vitro* and *in vivo* applications. Owing to the strong affinity of the gold-sulfur (Au-S) bond and physical absorption, Au offers ease of conjugation to various biological molecules (antibodies, DNA and peptide) that have been widely used in sensing, molecular imaging and drug targeting (Xie et al., 2010).

Instead of the classic AuNP, many other forms of Au nanostructures have been reported such as nanorods (Cabada et al., 2012, Murphy et al., 2005), nanospheres (Daniel and

Astruc, 2004), nanoshells, nanoplate nanocages (Hu et al., 2006) and nanoframes. A great effort nowadays is done on gold nanoshells (GNS) as they offer tuneable LSPR from visible to near infrared (NIR) wavelength by adjusting the core-to-shell ratio. NIR, also referred to as "biological window", allows deep penetration into soft tissues as the absorption of light in blood and water is limited and the magnitude of scattering in tissues is relatively low. In 2003, localised temperature increment to 37.4 ± 6.6°C with metal nanoshell silica core was first reported by Halas group and showed interesting positive results (Hirsch et al., 2003). Photothermal conversion upon laser irradiation contributes to the localised hyperthermia that causes irreversible cell death. This process is confined to nanoparticles distributed area *via* three potential mechanisms: damage to the cell membrane, prompt protein denaturation and induce production of reactive oxygen species (ROS). Exploration on metal nanoshell against cancer cells has been done by numerous researchers as this approach offers very little complications to the surrounding cells and fast recovery to the damaged site.

Lately, multifunctional nanosystems that provide the combination of both chemo- and photothermal therapy with metal nanoshell were reported. Wu and colleagues designed a system conveying both chemo- and photothermal therapy using gold nanoshell silica core with liposome; the synergistic system had better as anticancer efficacy as compared to either treatment alone (Wu et al., 2011). Laser irradiation induces localised hyperthermia and simultaneously deforms the gold nanoshell. In turn, chemotherapeutic drug is released gradually, in controlled-release manner, into the cancer cells thus causing cell death. However, the said system by Wu and colleagues is not suitable for *in vivo* studies as there

was absence of target scheme such as antibodies or peptides. Instead of liposome, polymer nanoparticles with poly (lactic acid) and poly (lactic-co-glycolide) (Hao et al., 2015, Yang et al., 2009), which was synthesised as a core and template for chemotherapeutic drugs loading. Another multimodal treatment for cancer was done by Liu *et al.* with Au-coated silica nanorattles loaded with docetaxel (DTX), the treatment successfully induced a localised hyperthermia and delivered the drug into human liver carcinoma (HepG2) cells (Liu et al., 2011).

To date, there was no known investigation on mesoporous silica nanoparticles (MSNs) coated with a thin layer of gold. MSNs have been suggested as a suitable platform for biomedical applications as they are biocompatible and biodegradable. Significant efforts have been dedicated to the development of MSNs as they offer numerous advantages such as a large surface area and ordered mesoporous channels, allowing higher payload of fluorescent dye, peptide and drug. Also, the well-defined surface chemistry of MSNs allows direct functionalisation and thus targeting specific site and prolonging the circulation time in the body (Figure 1.1). A major advantage of MSNs is they hold a sustained slow drug release property (Owens et al., 2016, Tang et al., 2014) and the rate of drug release can be tuned unlike liposome and polymer nanoparticles, which exhibit a burst release of drug.

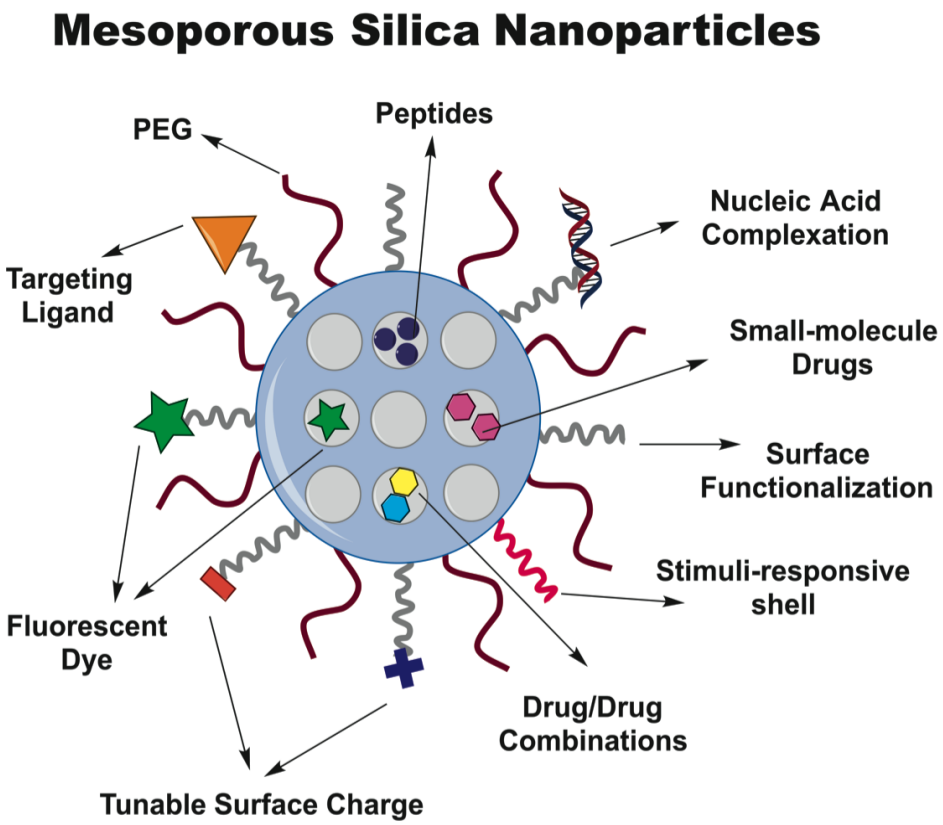

Figure 1.1: Multifunctional and cargo loading of mesoporous silica nanoparticles (MSNs). Adapted from Oupicky, 2014.

Many efforts have been made in designing nanodevices in recent years, however, most of the designed nanodevices offer only single cancer treatment that may lead to the incomplete eradication of cancer cells (Abbasian et al., 2017). Furthermore, traditional UV light-responsive nanodevices have been widely reported in literature but these nanodevices are not recommended for *in vitro* and *in vivo* applications. This owes to the UV light property that can cause the detrimental photochemical reactions and also has very limited tissue penetration depth (Olejniczak et al., 2015).

Herein, mesoporous silica nanoparticles (MSNs) coated with a layer of gold shell were synthesised for their multifunctionality including specific targeting, chemo- and photothermal therapy. Deformation of gold nanoshell upon two photon excitation (TPE) lead to localised temperature increment *via* photothermal conversion. At the same time, it allows the controlled release of the anticancer drug from the mesoporous silica core. Combination of both chemotherapy and photothermal therapy *via* multimodal nanoparticles promise a more comprehensive cancer treatment with minimal side effects on healthy cells.

1.1 Objectives of the study

1.1.1 General objectives

1. To synthesise, functionalise and characterise MSNs coated with a layer of gold shell (GNS).
2. To demonstrate two photon laser triggered gold nanoshell deformation *via* UV-VIS spectroscopy and TEM.
3. To evaluate the photothermal conversion efficacy of gold nanoshell.
4. To determine cytotoxicity of gold nanoshell in *in vitro* studies.

1.1.2 Specific objectives

1. MSNs, as a template for drug loading will be synthesised *via Stöber* process and it will then be covered by a layer of gold nanoshell by seed-mediated method to avoid premature release.

2. GNS surface will be functionalised with polyethylene glycol (PEG) followed by aptamer conjugation. The specificity of aptamer will be evaluated with two cell types.

3. GNS in aqueous solution will be excited with two photon laser and the final products will be collected and characterised.

4. Different concentration of GNS solution will be prepared and irradiated with 800 nm continuous wave (CW) laser as a proof-of-concept for 15 mins.

5. The toxicity of the DOX-GNS-PEG-Apt will be evaluated *via* cell meter^{TM} colorimetric cell cytotoxicity assay kit.

6. *In vitro* cytotoxicity effect of two photon excitation (TPE) induced gold nanoshell (GNS)-photothermal therapy (PTT) and control of drug release will be assessed.

CHAPTER 2

LITERATURE REVIEW

In this chapter, properties of gold nanoshell (GNS) followed by a brief introduction of the inner core, mesoporous silica nanoparticles (MSNs) will be introduced. The reasons behind MSNs gaining popularity for drug delivery will be discussed. Next, the target scheme on the GNS will be focused on aptamer. In addition, overview of doxorubicin (DOX) as well as the anti-tumour strategy will be described. Finally, the basic principle of two photon excitation (TPE) and its applications, such as controlled release and induced photothermal therapy (PTT), will also be reviewed.

Nanotechnology has made significant contributions to cancer therapy over the past several decades. Several nanoparticles such as Doxil, DaunoXome, Marqibo and Abraxaxane have been approved by Food and Drug Administration (FDA) for cancer treatment however, these nanoparticles are non-targeted delivery nanosystem which may eventually cause off target toxic effects (Smith, 2013). Thus, a tremendous efforts have been devoted to develop targeted drug delivery nanosystem and a number of these nanosystems for instance MM-302, BIND-014 and MBP-426 have been developed and are now in clinical trials (2016, 2014, Hrkach et al., 2012). Although these targeted nanomedicines appear to be very promising, these systems have the potential to cause the incomplete eradication of cancer cells as the designed nanomedicines offer only single cancer treatment, which is chemotherapy (Abbasian et al., 2017). Novel nanoparticles with targeting property and

synergistic therapeutic effects are demanded for more intensive and effective cancer therapy and hence, targeted GNS with synergistic chemo-photothermal therapy was designed in this work.

2.1 Gold nanoshells (GNS)

To date, there is a surge of interest in using a single sophisticated nanodevice for both diagnostic and therapeutic purposes. Spherical gold nanoparticles (AuNP) with excellent biocompatibility and optical properties had been incredibly conceived as the ideal contrast agents for oncological imaging and delivery vehicle for centuries. However, a major drawback of the conventional AuNP is its inability to shift the surface plasmon resonance (SPR) over a broad wavelength, thus limiting the uses of AuNP in medical applications. SPR is a physical process occurs when incident light at a specific angle, called resonance angle, hits the metallic surface causing the generation of optical properties. At present, different shapes of gold nanostructure such as cube, rod, disk and shell have been designed to overcome the shortness of spherical AuNP, which is the inability to shift the SPR over a broad wavelength. In recent years, there is a growing interest in using gold nanoshells (GNS) for targeted cancer therapies (Zhao et al., 2014). GNS was first invented by Halas group consisting a dielectric core surrounded by a controlled thickness of gold layer (Averitt et al., 1997). Gold-coated dielectric core particles are biocompatible and have outstanding molecular properties. Likewise, the SPR band generated can be easily tuned from visible to near infrared (NIR) wavelength through adjustments of the core/shell size ratio.

The tunable SPR of GNS over a wide region spectrum was first theoretically calculated and proposed by Neeves and Birnboim in 1989 (Neeves and Birnboim, 1988). Based on the calculation, a red shift of the spectrum would be expected as the shell thinned (Figure 2.1). This theory was then proved by Oldenburg *et al.* as 120 nm silica cores were prepared to generate GNS with shell thickness ranging from 20 to 33 nm $\pm$ 4 nm (Oldenburg et al., 1998). The ability to tune SPR of GNS from 520 nm to 800 nm (NIR region) where the biological tissues transparent window is located, offers tremendous opportunity in medical fields, including bio-imaging, biomolecular sensing and cancer therapy (Zhao et al., 2014). The ability of GNS to convert absorbed light into heat can kill cancer cells while addition of target scheme on the GNS promise nearby healthy tissues unharmed. Likewise, GNS is gaining popularity as it displays higher two photon induced photoluminescence (TPIP) which is appropriate for three dimensional *in vivo* fluorescence bio-imaging (Gao et al., 2011). This statement was supported by Park *et al.*, who found that a red shift of the spectrum would be expected as the shell thinned at brightness by TPIP of GNS is 140 times than fluorescent beads but slightly lower than gold nanorod (GNR) under the same condition (Park et al., 2008). Overall, GNS has opened up a new frontier in medical research especially in bio-imaging and drug delivery application.

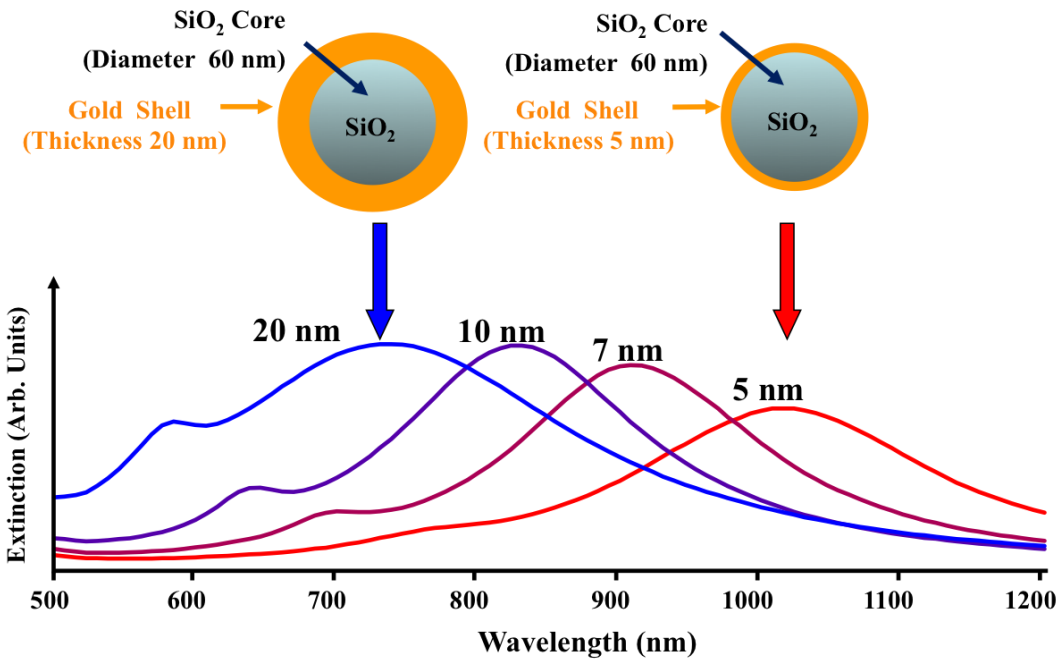

Figure 2.1: Theoretically calculated optical resonance of GNS over a range of core radius/shell thickness ratio. Adapted from Kim and Lee, 2015 and Loo et al., 2004.

GNS comprising a silica dielectric core have been extensively researched owing to both materials that are bioinert materials (Fay et al., 2015, Bear et al., 2013). Moreover, silica nanoparticle is preferred for use as this material is inexpensive, environmentally friendly, and easy to synthesise and functionalise. However, in this study, mesoporous silica nanoparticles (MSNs) will be facilitated as inner core instead of solid silica nanoparticles, which is more suitable for drug loading. In particular, MSNs-based drug carriers have been extensively reported in literature and the details will be covered in the following section.

2.2 Mesoporous silica nanoparticles (MSNs) as drug carriers

MSNs have gained substantial attention over the past few years. The synthesis, advantageous structural properties and recent progress in biomedical applications have been extensively discussed in literature, and is summarised in this subtopic.

Unlike solid silica nanoparticles, MSNs are porous material hence making MSNs suitable for further physical and biochemical modifications MSNs were first generated in 1992 by Kresge and co-workers. At that time, MSNs were known as mobile crystalline material-41 (MCM-41), which composed of a highly ordered pore arrangement and pore size ranging from 2 to 10 nm (Kresge et al., 1992). The invention of MSNs has overcome the shortcoming of the traditional formation of zeolite – the first known primitive porous material, which term coined in 1756 (Taboada et al., 2005). MSNs have been favourite raw materials in industry for several reasons: (1) large surface area whereby, > 700 m^2g^{-1} permits various modifications to be done (2) large pore volume enables high drug loading capacity for up to 200 - 300 mg in 1 g of silica (Bharti et al., 2015) (3) good biocompatibility (4) high chemical and thermal stability (5) low cytotoxicity (6) ease of functionalisation and (7) delivering variety of drugs in a controllable and sustainable manner. All these features make MSNs highly attractive for use in diverse biomedical applications: bioimaging, biosensing and drug delivery. MCM-41 introduced by Kresg *et al.* is not suitable for medical application due to the size of particle is too big and aggregation issue, which eventually hinder cellular uptake efficiency and causes vascular embolisation (Faraji and Wipf, 2009). Also, at cellular level, uptake of nanoparticle is size dependent with an optimum particle size of 100 nm is ideal for endocytosis (Xu et al.,

2012). For these reasons, enormous efforts have been devoted to utilise MSNs over solid silica nanoparticles and to synthesise MSNs in the nanometer range that is suitable for multimodal drug delivery.

In 2001, MSNs were employed as drug carrier by Vallet-Regi and coworkers for the first time (Vallet-Regi et al., 2001). In a particular study, ibuprofen which is a hydrophobic drug was loaded into the mesopores of MCM-41 with drug loading ratio of 30 % - by weight. It was also observed that 80 % of the loaded drug was released in a substantial manner within three days. Since then, delivering drug *via* MSNs has gained interests as reflected by an increase of research papers published while reporting MSNs as drug carriers. Another distinctive feature in supporting MSNs as drug carriers is the ability of MSNs to entrap both hydrophobic and hydrophilic drugs within their pores. Thus, the MSNs scaffold protect the encapsulated therapeutic drugs from direct enzymatic degradation in the process of drug delivery (Li et al., 2012b). At the same time, characteristics of on demand and time-controlled drug release are highly desirable. Hence, an MSN-based stimuli responsive system for controlling spatiotemporal release of drugs was designed to only exert an action at the desired target and time. In 2003, Lai and colleagues first proposed stimuli (chemical) responsive MSNs in which the opening pores were capped with cadmium sulfide (CdS) nanocrystals (Lai et al., 2003). The rapid release of drugs was observed only when the MSNs were exposed to thiol reducing agents (mercaptoethanol and dithiothreitol), both of which offset other pitfalls in the system and still cleaved the disulfide bond efficiently between MSNs and CdS (Figure 2.2). Likewise, zero premature release of drugs was recorded, thus the interaction between drugs and

normal healthy tissues during its circulation was minimised. This delivery system is particularly useful in delivering genotoxic drugs like chemotherapeutic drugs. Several stimuli other than chemical such as light, temperature and ultrasound, were also used to trigger drug release in a controlled manner. In this study, drug-loaded MSNs were covered by a layer of ultra-thin gold forming shell to avoid the premature release of drugs. Deformation of GNS occurred upon two photon excitation and subsequently release the drugs in a control manner. This approach will further be discussed in the later part of this chapter.

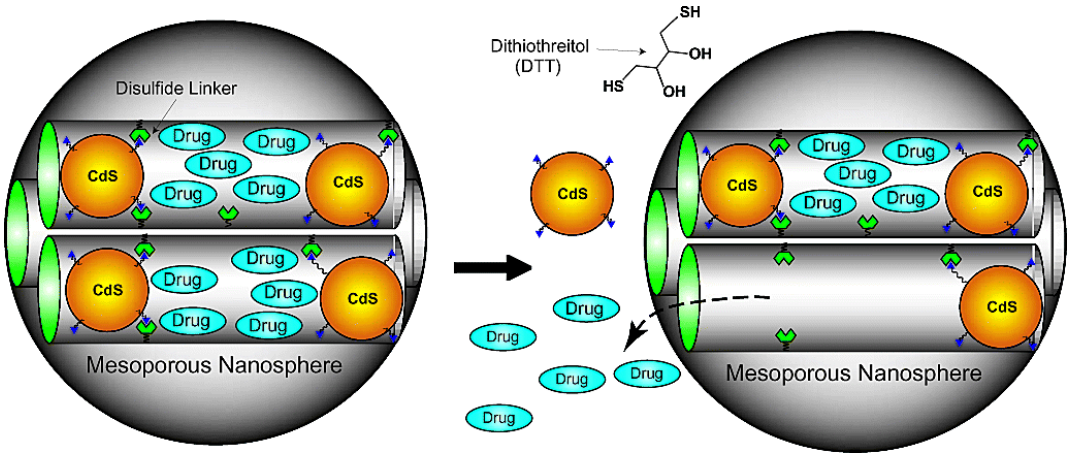

Figure 2.2: A controlled drug release nanosystem *via* chemical stimulus was designed. Adapted from Lai et al., 2003.

Up to this point, the characteristics and advantageous of MSNs and GNS have been discussed. For that matter, this study generated drug loaded MSNs with a thin layer of gold. The GNS in this study was also bio-functionalised; hence, the following section aptly describes integration of biospecificity features and selection of target scheme.

2.3 Target scheme - antibodies, peptide & aptamer (Apt)

The ideal goal of nanodevices for cancer therapy is to design a high target specificity and affinity delivery system, and to attain an effective therapeutic drug concentration to the tumour. Besides, untoward toxicity to the surrounding tissues, of which usually occur when utilising conventional chemotherapy, can be minimised with targeted delivery system. Thus, the use of targeted-nanodevices may increase the effectiveness of nanoparticle homing. Generally, there are two major targeting schemes: passive and active targeting mechanisms (Chakraborty et al., 2011). Passive targeting refers to the accumulation of nanodevice at cancer tissues based on the body's natural biological response toward pharmacological physiological or physicochemical factors of the devices (Shahbazi et al., 2012). This passive targeting, however, lacks selectivity in the mechanism of action. Alternatively, active targeting nanodevices can efficiently bind to target sites over the surrounding tissues thus, avoiding undesirable toxicity issues (Choi et al., 2010). This approach facilitates specific interaction between target moieties (antibodies, peptides, aptamer (Apt), sugar and small molecules) with either receptors or antigens that are overexpressed on cancer cell surface (Kumari et al., 2015, Fenart et al., 1999). Of these moieties, monoclonal antibodies with high affinity and specificity have been the gold standard in targeted cancer therapy (Zito et al., 2016). Nonetheless, numerous problems when using antibodies-based therapy include large size of the antibody, high production cost and undesired immunogenicity that limit their use in medical field (Chames et al., 2009). As a consequence, relatively new target binding technology called aptamer has becoming a valuable alternative in targeted cancer therapy.

2.3.1 Aptamer (Apt)

Nowadays, aptamer (Apt) have been a major focus of interest for bio-imaging, gene therapy and drug delivery applications. This owes to Apt's inherent similarities but with more advantages over traditional antibodies like high affinity and specificity to target receptors or antigens, but at a fraction of the size. In 1990, Apt was first discovered by Ellington & Szostak and Tuerk & Gold as RNA ligands that were designed to selectively bind to T4 DNA polymerase and organic dyes, respectively (Tuerk and Gold, 1990, Ellington and Szostak, 1990). Apt is made up of either single-stranded RNA or DNA and is folded into three-dimensional conformations (Figure 2.3).

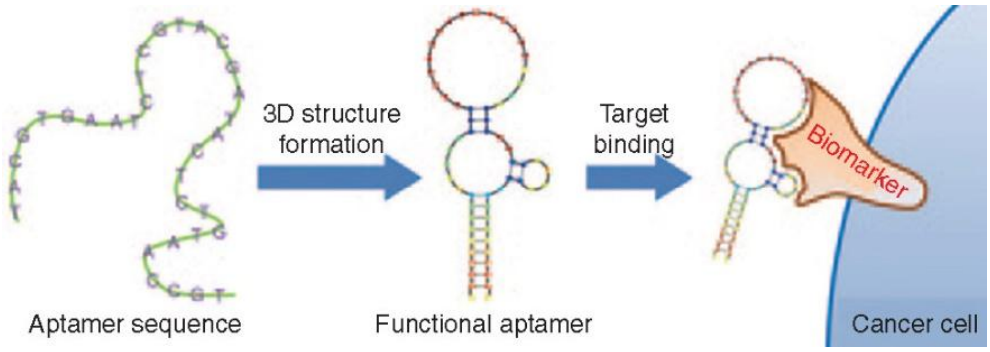

Figure 2.3: Schematic diagram of Apt folded into three-dimensional conformations. Adapted from Sun et al, 2014.

They are more economical and easier to prepare as the recipes do not involve cell culturing and animals uses. Furthermore, unlike antibodies, which undergo denaturation easily at higher temperature, Apt is thermodynamically stable, making it suitable to use at varying temperature for *in vitro* and *in vivo* studies. Moreover, Apt which usually are 20 - 60 nucleotides long, are 20 - 25 times smaller than monoclonal antibodies. At such size, Apt may perform better and penetrates tumour deeper thus becoming ideal therapeutic agent

against cancers (Xiang et al., 2015, Zhu et al., 2012). Additionally, it is nearly impossible to design antibodies with no immunogenicity as they are often derived from animals like mouse, rabbit, donkey or even with humanised antibodies. In contrast, Apt is synthetic oligonucleotides that are not recognised as foreign bodies by immune system, and therefore immune response is avoided.

In 2004, the first Apt-targeted drug delivery system was reported by Farokhzad *et al.* (Farokhzad et al., 2004). The drug-loaded nanoparticles (NPs) incorporated with A10 prostate-specific membrane antigen (PSMA) Apt for targeting PSMA protein overexpressed on prostate cancer epithelial cells. After 16 hours incubation of A10 PSMA Apt conjugated NPs in both prostate LNCaP and PC3 cell lines, the binding of the NPs was clearly noticeable in LNCaP cell line but not in PC3 cell line as PC3 cell line does not express PSMA protein. For another example, an MUC1 Apt-doxorubicin (DOX) complex was designed by Hu and colleagues in 2012 for selectively delivering chemotherapy drugs to liver (HepG2) and lung (A549) cancer cells (Hu et al., 2012). The reduction of cell viability to nearly 70 % and 80 % for HepG2 and A549 cancer cells respectively was witnessed in this particular study. Also, this study demonstrated that the MUC1 Apt alone was not cytotoxic towards either cell lines.

Among Apt, AS1411 Apt is the first to enter clinical trial (Bates et al., 2009). AS1411 Apt, contains 26 bases with guanine rich sequence targeting nucleolin proteins, which is predominantly found on plasma membrane of most cancer cells. AS1411 Apt exerts anti-

proliferative effect and does so by inhibiting the binding of nucleolin to bcl-2 mRNA (Aravind et al., 2012, Bates et al., 2009). Therefore, a number of nanocarrier systems conjugated with AS1411 Apt were designed as they promote cellular internalisation by interacting with nucleolin protein. This inhibition process matters because stabilisation of bcl-2 mRNA when bound to nucleolin stops cells from undergoing apoptosis, thus leading to the overproduction of cancer cells (Soundararajan et al., 2008, Otake et al., 2007, Derenzini et al., 1995). Interaction of AS1411 Apt with nucleolin at the plasma membrane and later endocytosed intracellularly would leave bcl-2 mRNA dangling, which eventually unlocking the apoptotic pathway (Fogal et al., 2009).

2.4 Doxorubicin

In the present study, combination of both chemo-photothermal therapy can be achieved with this synthesised gold nanoshell with mesoporous silica core (GNS) by co-loading chemotherapeutic drugs, doxorubicin (DOX) into mesoporous channel. DOX which is also named as Adriamycin, has molecular formula $C_{27}H_{29}NO_{11}$ and molecular weight of 543.52 g/mol. Figure 2.4 shows its chemical structure; it consists of four-membered ring systems and a link with an aminoglycoside *via* glycosidic bond at ring atom 7 (Cutts et al., 2005).

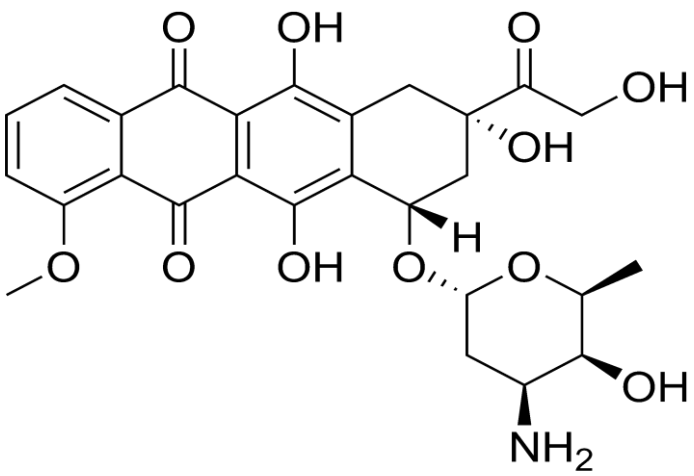

Figure 2.4: Chemical structure of Doxorubicin (DOX). Adapted from Cacycle, 2018.

DOX is isolated from actinobacteria called *Streptomyces peucetius* by mutating a daunomycin-producing strain and the produced DOX is then classified as a member of anthracycline family. Its chemotherapeutic potential for cancer treatment was first reported by Arcamone *et al.* in 1969 (Arcamone et al., 2000). In the meantime, Di Marco and co-workers proved DOX to have better therapeutic index when compared to daunorubicin, which is the precursor of DOX (DiMarco et al., 1969). In early 1970s, anti-tumour efficiency of DOX had been evaluated in clinical trials and DOX was recognised as one of the most effective chemotherapeutic drugs (O'Bryan et al., 1973, Tan et al., 1973, Middleman et al., 1971). Within a few years DOX was approved by United States FDA for medical use. To date, DOX is still considered a mainstay chemotherapeutic drug due to its excellent anti-tumour efficacy against various type of cancers including Hodgkin's lymphoma, breast-, ovarian-, lung-, liver- and thyroid cancer among others. Several mechanisms have been proposed for DOX-mediated anti-tumour effects: (1) intercalation between adjacent GC base pairs in DNA double helix, (2) inhibition of topoisomerase II activity and (3) induction of reactive oxygen species (ROS) production. These

mechanisms elicit DNA damage, leading to the activation of downstream targets that regulates apoptosis or cell cycle arrest.

Despite DOX broad and promising applications in chemotherapy, the clinical use of doxorubicin is limited by indiscriminative toxic side effects as DOX is distributed into tissues and intracellular compartments *via* systemic circulation. Administration of DOX at cumulative doses $\geqslant$550 mg/m^2 is associated with an increased incident of cardiac failure among cancer patients (Rahman et al., 2007). However, the exact molecular mechanism by which DOX inducing cardiomyopathy is still unclear. To overcome the indiscriminative toxic side effects associated with previous formulations, Doxil was developed and approved by United Stated FDA in 1995. Doxil, a formulation of doxorubicin encapsulated in liposomes was the first nanodrug used to treat several cancers including ovarian cancer, AIDS-related Kaposi's sarcoma, and multiple myeloma (Barenholz, 2012). This new formulation had a successful increased of the survival rate and at the same time, reduced toxicity to the surrounding tissues. Nonetheless, administration of this nanodrug did not show a pronounced clinical efficacy in cancer treatment (Seynhaeve et al., 2013). Furthermore, the surface of this nanodrug was not functionalised with any targeting ligand and thus, provide the possibility of delivering the DOX to the healthy cells (Gao and Jiang, 2017). In short, nanodrugs with specific target and controlled release properties are essential to improve the clinical efficacy while sparing normal healthy cells.

2.5 Principle of two-photon excitation (TPE)

The foundation of two-photon excitation (TPE) ideation was first proposed by Maria Goppert-Mayer in 1931 (Göppert-Mayer, 1931) however, this photophysical properties had not been practically tested until 1960s when laser with high photon intensities was invented (Kaiser and Garrett, 1961). Prior to further explanation about TPE, the knowledge on conventional single photon excitation needs to be understood. Single photon excitation is a linear process as it involves the direct transition of electron from fluorophore between ground and excited state by single photon in the Ultraviolet illumination. In contrast, TPE fluorescence accomplished the transition of electron from fluorophore between two electronic states by the almost simultaneous absorption of two photons (Oheim et al., 2006). Two photon absorption is considered as a nonlinear process where the first photon promoted an electron to virtual state and eventually brought to the excited state by the second photon (So et al., 2000). These can be explained using quantum theory, the energy of a photon is inversely proportional to its wavelength, thus, two photon should have a wavelength increased by a factor of two, to attain equivalent transition state excited with single photon (Benninger and Piston, 2014). As a result, fluorophore can be excited with long wavelength (infrared region) too other than short wavelength (ultraviolet) (Rocheleau and Piston, 2001). These concepts are summarised in Figure 2.5.

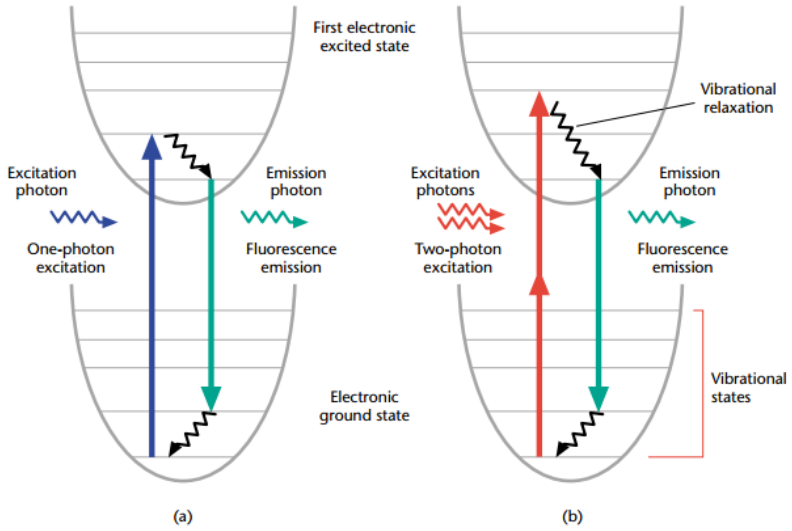

Figure 2.5: Jablonski (energy level) diagram of (a) single photon excitation and (b) two photon excitation. Adapted from So, 2002.

In the present study, two-photon laser was employed to induce localised photothermal therapy (PTT) and simultaneously deforms the gold nanoshell (GNS) for the controlled release of DOX. Two photon laser is highly recommended in biological experiments as low average excitation power is needed and therefore, the degree of photodamage on biological specimen can be reduced (Hopt and Neher, 2001). Moreover, TPE exerts a deeper tissue penetration making it as a superior alternative to single photon laser. Additionally, the nonlinearity photon absorption of TPE permits the activation of GNS restricted to the focal point of the laser beam (Shen et al., 2016). This offers precise spatial control of GNS activation during cancer treatment, eventually minimising the off-target drift damage to the surrounding normal healthy tissues.

2.5.1 Photothermal therapy (PTT)

One of the key elements in regulating the fate of biological systems ranging from single cell to tissues and organisms is temperature. Elevation of temperature above normal body temperature could lead to irreversible cell damage, and even vital organ dysfunction. On the brighter side, increase of temperature above normal (hyperthermia) in a control manner could be applied to get rid of undesired cancer cells. Thus, extensive efforts have been devoted to the development of novel nanoplatforms for controlled and localised hyperthermia in target area, while leaving nearby healthy tissues unharmed (Tsai et al., 2018, Pattani and Tunnell, 2012, Gutwein et al., 2012). A promising technique to achieve controlled and localised hyperthermia is laser-induced photothermal therapy (PTT) (Mendes et al., 2017). Among all nanoparticles, gold nanoparticles (AuNP) are the most studied PTT materials due to excellent heat generation *via* non-radiative processes (Abadeer and Murphy, 2016). Non-equilibrium heat is established when electron of AuNP was photoexcited at incident photon. The relaxation of excited electron *via* electron-electron scattering leading to the rapid temperature increment at the AuNP surface. The heat energy from electron is transferred to photon as a consequence of electron-photon collision and thermal equilibrium is reached (Link and El-Sayed, 2000). Lastly, AuNP is cooled down by dissipating the heat to surrounding medium *via* photon-photon interaction. The overall process of light induced thermal effect is summarised in Figure 2.6.

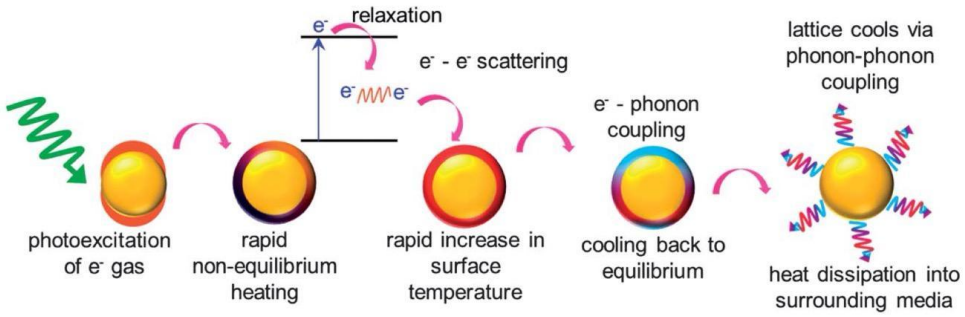

Figure 2.6: The overall process of photo-thermal conversion upon laser irradiation. Adapted from Webb and Bardhan, 2014.

Gold nanoshells (GNS) are especially attractive for PTT because of their tunable plasmon resonance fall into the near infrared (NIR) region, where most of the biological tissues are relatively transparent to light in NIR region. The GNS mediated PTT in breast cancer cells was first performed by Hirsch *et al.* in 2003 (Hirsch et al., 2003). The loss of Calcein AM fluorescence in GNS treated group indicates cell damage after NIR laser irradiation. This phenomenon was not observed in control group with laser irradiation alone. The same group carried out a study in 2005 demonstrating dual imaging and NIR thermal therapy approach with GNS (Loo et al., 2005). This time, GNS was conjugated to either non-specific antibodies or anti-HER2 antibodies and subsequently incubated in HER2-positive SKBr3 breast cancer cells. SKBr3 breast cancer cells incubated with anti HER2-conjugated GNS underwent apoptosis within laser spot after NIR (820 nm) irradiation treatment for 7 minutes with output of 0.008 W/m^2.

In the following year, two cell types, SKBr3 breast cancer cells and HDF human dermal fibroblast (HER2 negative) were seeded side by side followed by incubation with HER2-